

## Nonohmic Behavior of SnO<sub>2</sub>.MnO<sub>2</sub>-Based Ceramics

Marcelo O. Orlandi, Paulo Roberto Bueno\*, Edson Roberto Leite, Elson Longo

Laboratório Interdisciplinar de Eletroquímica e Cerâmica,  
Universidade Federal de São Carlos, Departamento de Química,  
C.P. 676, 13560-000 São Carlos - SP, Brazil

Received: December 4, 2002; Revised: February 1, 2003

The present paper describes the nonohmic behavior of the SnO<sub>2</sub>.MnO-based system and analyzes the influence of the sintering time and the Nb<sub>2</sub>O<sub>5</sub> concentration on this system's electrical properties. A nonlinear coefficient of ~7 was obtained for a 0.2 mol%-doped Nb<sub>2</sub>O<sub>5</sub> composition, which is comparable to other values reported in the literature for the ternary SnO<sub>2</sub>-based systems.

A recent barrier formation model proposed in the literature to explain the nonlinear electrical behavior of SnO<sub>2</sub>-based systems is used to clarify the role of the MnO constituent in the formation of the barrier, taking into account the influence of segregated atoms, precipitated phase and oxygen species in the grain boundary region.

**Keywords:** SnO<sub>2</sub>, varistor, semiconductor

### 1. Introduction

Our research group has discovered a class of polycrystalline nonohmic devices composed predominantly of SnO<sub>2</sub><sup>1</sup> and, since this discovery, we have been engaged in exhaustive studies involving this class of ceramic materials<sup>2,3-8</sup>.

Although SnO<sub>2</sub> is normally used in devices made of porous materials such as gas sensors<sup>9,10</sup>, the addition of CoO and MnO<sub>2</sub> to SnO<sub>2</sub> produces high densification<sup>11,12</sup>, allowing for the development of other electronic devices such as varistors<sup>1-8,13</sup>. However, most of the nonlinear electrical behavior of these ceramics has been obtained in the SnO<sub>2</sub>.CoO-based systems<sup>1-8,13</sup>. Yongjun *et al.*<sup>14</sup> have demonstrated that CoO can be replaced by ZnO without significantly altering the nonlinear coefficient ( $\alpha$ ) when compared to the original SnO<sub>2</sub>.CoO-based system, the first of such SnO<sub>2</sub>-based systems reported on in the literature<sup>1</sup>. Castro *et al.*<sup>11</sup> have also shown how dopants such as Co<sub>3</sub>O<sub>4</sub>, CuO, MnO<sub>2</sub>, Bi<sub>2</sub>O<sub>3</sub> and Sb<sub>2</sub>O<sub>3</sub> can influence the dielectric properties, microstructure and densification of SnO<sub>2</sub>-based ceramics.

The main goal of this work is demonstrate that it is also possible to produce good nonlinear electrical properties in SnO<sub>2</sub>.MnO-based systems such as the ones present in SnO<sub>2</sub>.CoO and SnO<sub>2</sub>.ZnO. An investigation was also made of the influence of the Nb<sub>2</sub>O<sub>5</sub> concentration and sintering time on the nonlinear electrical behavior of the SnO<sub>2</sub>.MnO-based system.

### 2. Experimental Procedure

The ceramic samples used in this study were prepared using the ball milling process in an alcohol medium. The oxides used were SnO<sub>2</sub> (Merck), MnO<sub>2</sub> (Aldrich), and Nb<sub>2</sub>O<sub>5</sub> (CBMM). The composition of the molar system was (99.5-X)% SnO<sub>2</sub> + 0.5% MnO<sub>2</sub> + X% Nb<sub>2</sub>O<sub>5</sub>, with X being 0.05; 0.10; 0.15 and 0.2% (SMNbX). The chemical analysis of SnO<sub>2</sub> revealed that the main impurities were Pb (< 0.01%), Fe (< 0.01%), Ge (< 0.005%) and Cu (< 0.005%), all in mol%. The powder obtained was pressed into pellets (9.0 mm × 1.0 mm) by uniaxial pressure (~1.5 MPa), followed by isostatic pressure at 150 MPa.

The sintering temperature was determined after a linear shrinkage and linear shrinkage rate study as a function of temperature, using a NETZCH 402E dilatometer at a constant heating rate of 10 °C/min up to 1450 °C in an ambient atmosphere.

The pellets were sintered at 1300 °C for 1, 2 and 4 h. The heating and cooling rates used were 10 °C/min. The tetragonal structure of SnO<sub>2</sub> (rutile structure) was confirmed as the single phase by X-ray diffraction (SIEMENS Model D-5000) on the mixed powder. The mean grain size of the samples was determined based on an analysis of SEM micrographs (ZEISS DSM 940A), following the ASTM E112-88 standard. The microstructures were also characterized by an X-ray energy dispersive spectroscopy (EDX)

\*e-mail: paulo@iris.ufscar.br

stage attached to the scanning electron microscope.

For the electrical measurements, the two faces of the samples were coated with silver paste, after which the pellets were heat treated at 300 °C for 30 min. Current-tension measurements were taken using a High Voltage Measure Unit (KEITHLEY Model 237). The nonlinear coefficient ( $\alpha$ ) was obtained by linear regression on a logarithmic scale of around 1 mA/cm<sup>2</sup> and the breakdown electric field ( $E_b$ ) was obtained at this current density.

### 3. Results and Discussion

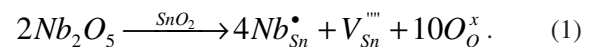
The tetragonal structure of SnO<sub>2</sub> (rutile structure) was confirmed as the single phase by X-ray diffraction (SIEMENS Model D-5000) on the mixed powder. Figure 1 shows the X-ray diffraction patterns (XRD) of the samples studied, indicating that only the cassiterite phase deriving from the SnO<sub>2</sub> is present, as has been observed in other reports on SnO<sub>2</sub>.CoO-based systems<sup>1,8,11</sup>.

Figure 2 shows the linear shrinkage rates for the systems studied. A mass transport mechanism is visible, leading to densification at temperatures ranging from approximately 1000 to 1350 °C, which is probably the same process discussed by Cerri *et al.*<sup>11</sup>. This densification process was attributed to mass transport through the grain boundary caused by oxygen vacancies. The inset of Fig. 2 shows that the increase of Nb<sub>2</sub>O<sub>5</sub> doping concentration caused a reduction of the linear shrinkage rate.

Figures 3 and 4 illustrate the typical SEM micrographs found in SMNb0.05% and SMNb0.2% sintered for different lengths of times. These SEM micrographs reveal that the microstructure produced in SnO<sub>2</sub>.MnO-based systems is similar to that obtained in SnO<sub>2</sub>.CoO-based ceramic sys-

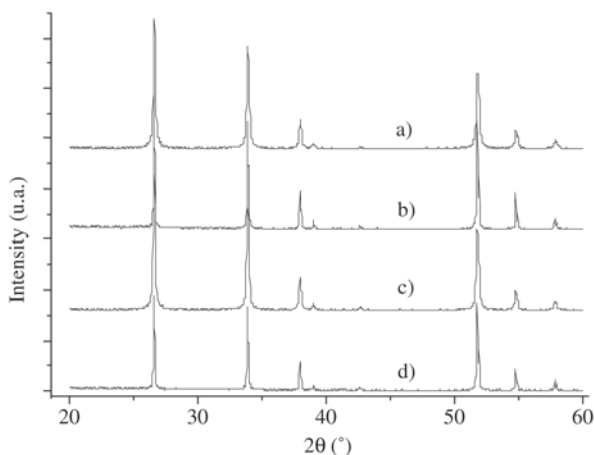
tems<sup>1-8,13</sup>. However, a precipitate was clearly observed in some of the SEM micrographs, mainly when higher concentrations of Nb<sub>2</sub>O<sub>5</sub> were present, as shown in Fig. 4b and as discussed in Ref. 15. The evidence indicates that this precipitated phase is rich in Mn and oxygen.

Table 1 lists the mean relative density obtained for each sintered sample. The mean grain size ( $d$ ) increased in all the systems as with longer sintering times due to the coalescence of grains in the final sintering stage. The  $d$  values showed a tendency to decrease with increasing concentrations of Nb<sub>2</sub>O<sub>5</sub> doping. This finding suggests that higher concentrations of Nb<sub>2</sub>O<sub>5</sub> cause greater precipitation of Mn at the grain boundary in SnO<sub>2</sub>.MnO-based systems, thereby hindering sintering and densification. Our EDX analysis revealed that Nb<sub>2</sub>O<sub>5</sub> is homogeneously distributed on this polycrystalline ceramic and that, similarly to the SnO<sub>2</sub>.CoO-based system<sup>1-8,13</sup>, it forms a solid-state solution with SnO<sub>2</sub>, as illustrated below:



Thus, since Nb<sub>2</sub>O<sub>5</sub> forms a solid solution, it may cause Mn precipitation when present in higher concentrations. Similarly to the SnO<sub>2</sub>.CoO-based system<sup>1,6</sup>, Nb<sub>2</sub>O<sub>5</sub> is also responsible for grain conduction, while Mn segregation and/or precipitation is responsible for grain boundary resistance and potential barrier formation, based on the model proposed<sup>4,15</sup>.

Table 2 lists the nonlinear coefficient ( $\alpha$ ) and breakdown electric field ( $E_b$ ) obtained for the SnO<sub>2</sub>.MnO-based systems, as well as the influence of sintering time on the non-



**Figure 1.** XRD patterns of SnO<sub>2</sub>.MnO-based systems sintered at 1300 °C for 4 h. a) SMNb0.05%; b) SMNb0.10%; c) SMNb0.15%; d) SMNb0.20%.

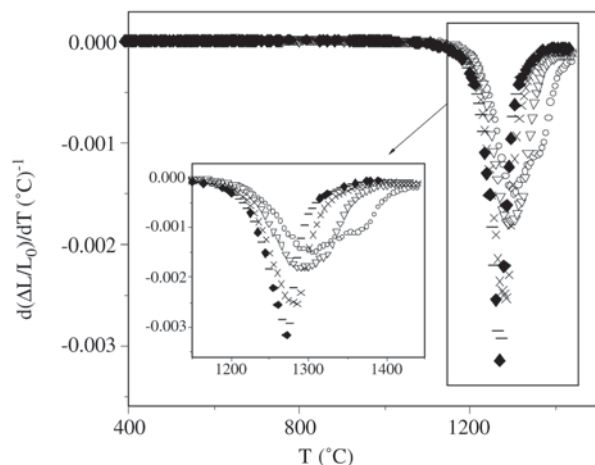


**Figure 2.** Linear shrinkage rate as a function of temperature for the concentrations of Nb<sub>2</sub>O<sub>5</sub> (mol%): (◆) 0.05%; (×) 0.10%; (∇) 0.15%; and (○) 0.20%

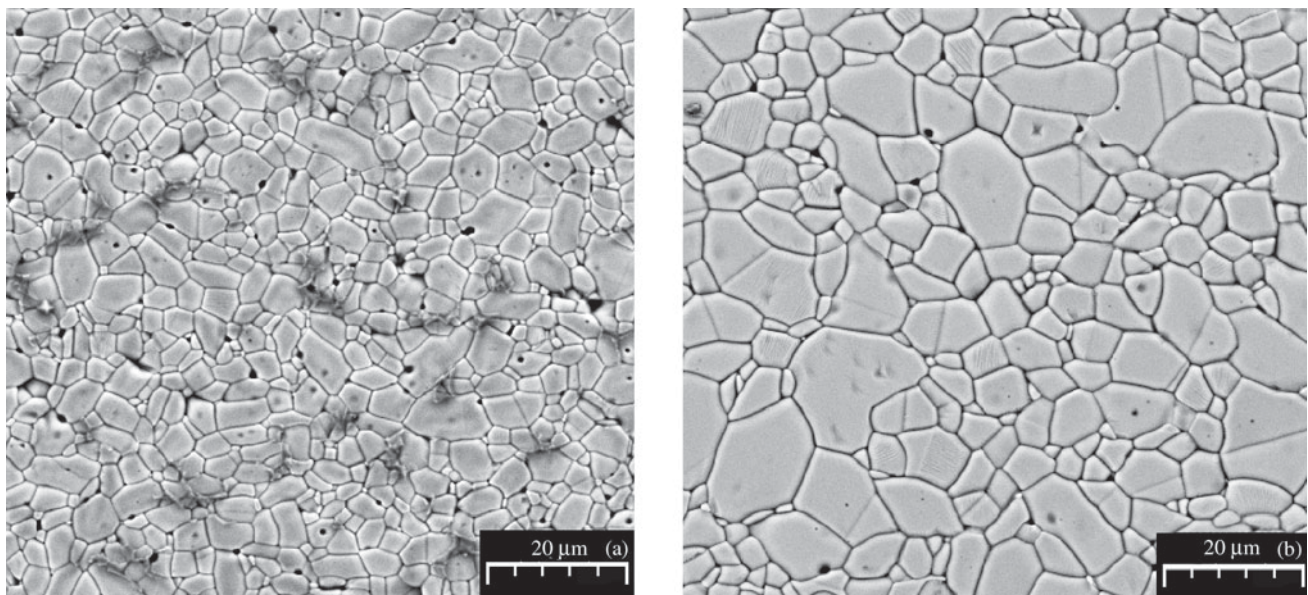


**Figure 3.** SEM micrographs of the SMNb0.05% composition sintered at 1300 °C for: (a) 1 h; (b) 4 h.

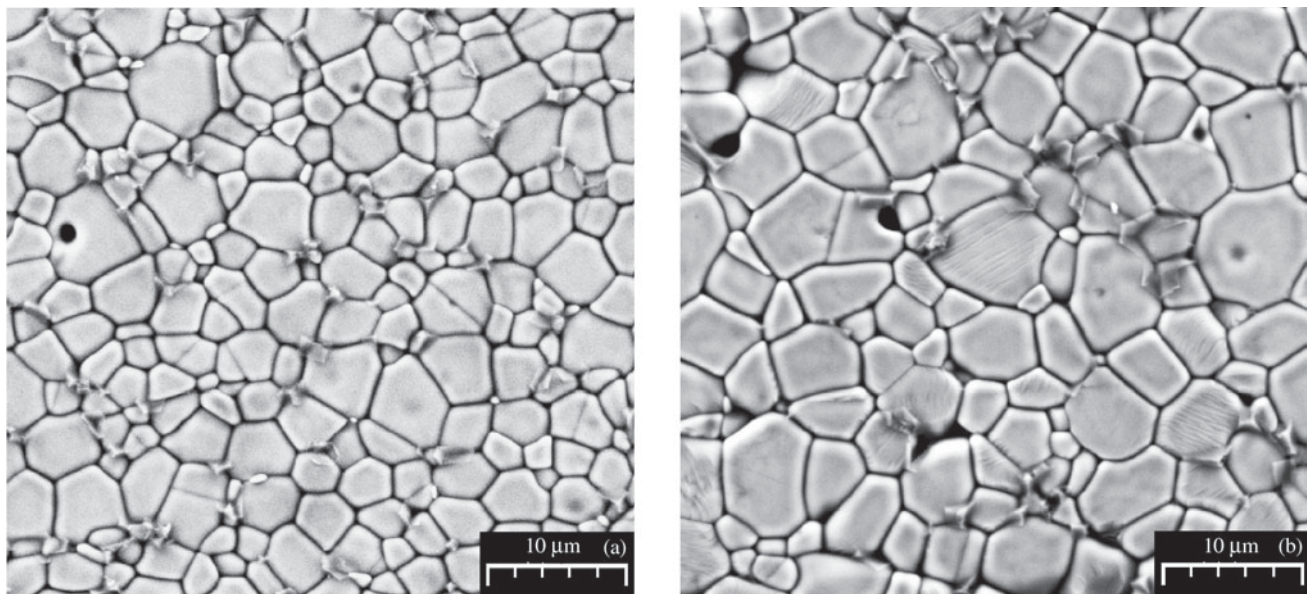


**Figure 4.** SEM micrographs of the SMNb0.2% composition sintered at 1300 °C for: (a) 1 h; (b) 4 h.

**Table 1.** Mean grain size ( $d$ ) and relative density values ( $\rho_r$ ) for the  $\text{SnO}_2\text{-MnO}_2$ -based varistor system with varying sintering times

System	Sintering Time (h)					
	1		2		4	
	$d$ (mm)	$\rho_r$ (%)	$d$ (mm)	$\rho_r$ (%)	$d$ (mm)	$\rho_r$ (%)
SMNb0.05%	4.3	98.4	5.7	97.7	6.7	97.9
SMNb0.10%	4.7	97.0	5.7	98.1	8.0	99.1
SMNb0.15%	3.3	98.4	4.9	99.1	6.8	98.9
SMNb0.20%	2.4	98.8	3.7	99.3	5.5	98.7

linear electrical properties of this varistor system. Figure 5 illustrates the characteristic  $I$ - $V$  curves as a function of  $\text{Nb}_2\text{O}_5$  for systems sintered for 2 h. As shown in Table 2, the  $\alpha$  and  $E_b$  values remained unchanged with sintering time in the SMNb0.05% samples. However, the other systems showed a decrease in the  $\alpha$  and  $E_b$  values as the sintering time increased. The reduction of the  $\alpha$  value with sintering time in the SMNb0.15% and SMNb0.20% samples may have resulted from the more heterogeneous microstructure and composition of the grain boundary region, as suggested by the SEM micrographs in Fig. 4. The heterogeneity of the grain boundary was likely formed by Mn segregated atoms as well as by the presence of a new precipitated Mn-rich phase. The presence of precipitated phases and the increase in mean grain size possibly caused a less effective potential barrier throughout the microstructure, which is responsible for decreasing the breakdown voltage and increasing the leakage current.

The best  $\alpha$  values were recorded for the SMNb0.2% samples, mainly those sintered for 1 h, which presented a value of  $\sim 7$ . This value is comparable to those reported in other references, such as Refs. 1, 3 and 6 for  $\text{SnO}_2$ .CoO-based systems doped with 0.05 mol% of  $\text{Nb}_2\text{O}_5$  and for  $\text{SnO}_2$ .ZnO-based systems<sup>14</sup>. We believe that the addition of a small amount of  $\text{Cr}_2\text{O}_3$  may improve the nonlinear electrical properties, as is the case of the  $\text{SnO}_2$ .CoO-based system reported on in Ref. 3. The addition of  $\text{Cr}_2\text{O}_3$  to the  $\text{SnO}_2$ .MnO-based system will therefore be the subject of future work.

The present work demonstrates that it is possible to develop nonohmic properties in  $\text{SnO}_2$ .MnO-based systems such as  $\text{SnO}_2$ .CoO- and  $\text{SnO}_2$ .ZnO-based systems. All these systems, doped with only small concentrations of  $\text{Nb}_2\text{O}_5$  (0.05 mol%), display a values of  $\sim 7$  to  $24$ <sup>1,6,13,14</sup>. Our research group recently demonstrated that this system's nonohmic behavior derives from the existence of a potential Schottky-type barrier at the grain boundary<sup>7</sup> similar to the barrier found in traditional ZnO-based systems. Furthermore, we have shown that the nonohmic properties of  $\text{SnO}_2$ -based varistor systems are dependent on an atmosphere treatment<sup>5,13</sup>. The sum of these characteristics and the similarity

of the nonlinear electrical behavior observed in different  $\text{SnO}_2$ -based systems suggest that the formation of the potential barrier is similar in all these  $\text{SnO}_2$ -based systems<sup>15</sup>. These findings, moreover, agree with the barrier formation mechanism model we proposed and discussed in a recent article<sup>5,7,13,15</sup>.

It is important to emphasize here that, since there are Co, Zn and Mn atoms segregated (and some of them also precipitated) at the grain boundary (which is a highly nonstoichiometric region of the material) of these  $\text{SnO}_2$ -based systems, defects such as  $\text{Co}_{\text{Sn}}''$ ,  $\text{Zn}_{\text{Sn}}''$ ,  $\text{Mn}_{\text{Sn}}''$  or  $\text{Mn}'_{\text{Sn}}$  will give rise to  $V_{\text{Sn}}''''$  in grain boundaries and, hence, generate excess oxygen in this region, as discussed in detail in Refs. 4, 5 and 15.

#### 4. Conclusions

In conclusion, the present work discussed a new composition based on  $\text{SnO}_2$ .MnO doped with  $\text{Nb}_2\text{O}_5$ , whose nonohmic behavior was similar to that reported on in the literature for other ternary systems. The  $\alpha$  and  $E_b$  values remained constant with variable sintering times in the system doped with 0.05 mol% of  $\text{Nb}_2\text{O}_5$  but decreased in com-

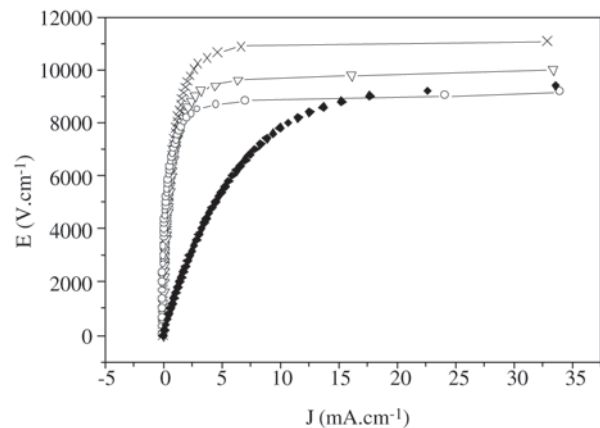


**Figure 5.**  $I$ - $V$  characteristic curves of compositions sintered for 2 h. ( $\blacklozenge$ ) 0.05%; ( $\times$ ) 0.10%; ( $\nabla$ ) 0.15%; ( $\circ$ ) 0.20%.

**Table 2.**  $\alpha$ ,  $E_b$  and values for the  $\text{SnO}_2$ .MnO<sub>2</sub>-based varistor system with different sintering times.

System	Sintering Time (h)					
	1		2		4	
	$\alpha$	$E_b$ (V.cm <sup>-1</sup> )	$\alpha$	$E_b$ (V.cm <sup>-1</sup> )	$\alpha$	$E_b$ (V.cm <sup>-1</sup> )
SMNb0.05%	1.3	900	1.4	1600	1.5	1530
SMNb0.10%	2.5	7060	3.7	7610	3.4	8860
SMNb0.15%	4.1	8500	4.0	6950	3.5	4640
SMNb0.20%	7.3	9350	5.8	7100	4.1	4900

positions containing higher concentrations of Nb<sub>2</sub>O<sub>5</sub>. The latter behavior was attributed to an increase of mean grain size and to microstructural heterogeneity (mainly in the grain boundary region), which generated higher leakage current values. The best nonohmic behavior was found in the samples doped with 0.20 mol% of Nb<sub>2</sub>O<sub>5</sub>, whose  $\alpha$  value was  $\sim 7$ .

### Acknowledgements

The financial support of this research by CNPq, FINEP, PRONEX and FAPESP (all Brazilian research funding institutions) is gratefully acknowledged.

### References

1. Pianaro, S.A.; Bueno, P.R.; Longo, E.; Varela, J.A. *J. Mat. Sci. Lett.*, v. 14, p. 692, 1995.
2. Antunes, A.C.; Antunes, S.R.M.; Pianaro, S.A.; Longo, E.; Leite, E.R.; Varela, J.A. *J. Mat. Sci.: Mat. Electron.*, v. 12, p. 69, 2001.
3. Bueno, P.R.; Pianaro, S.A.; Pereira, E.C.; Bulhões, L.O.S.; Longo, E.; Varela, J.A. *J. Appl. Phys.*, v. 87, n. 7, p. 3700, 1998.
4. Bueno, P.R.; Cassia-Santos, M.R.; Leite, E.R.; Longo, E.; Bisquert, J.; Garcia-Belmonte, G.; Fabregat-Santiago, F. *J. Appl. Phys.*, v. 88, p. 6545, 2000.
5. Cassia-Santos, M.R.; Bueno, P.R.; Longo, E.; Varela, J.A. *J. Eur. Ceram. Soc.*, v. 21, p. 161, 2001.
6. Pianaro, S.A.; Bueno, P.R.; Olivi, P.; Longo, E.; Varela, J.A. *J. Mat. Sci. Lett.*, v. 16, p. 159, 1997.
7. Pianaro, S.A.; Bueno, P.R.; Olivi, P.; Longo, E.; Varela, J.A. *J. Mat. Sci.: Mat. Electron.*, v. 9, p. 158, 1998.
8. Pianaro, S.A.; Bueno, P.R.; Longo, E.; Varela, J.A. *Ceram. Intern.*, v. 25, n. 1, p. 1, 1999.
9. Fagan, F.G.; Amararakoon, V.R.W. *J. Am. Ceram. Soc.*, v. 72, n. 3, p. 119, 1993.
10. Jarzebski, Z.M.; Marton, J.P. *J. Electrochem. Soc.*, v. 123, p. 299C, 1976.
11. Cerri, J.A.; Leite, E.R.; Gouvea, D.; Longo, E. *J. Am. Ceram. Soc.*, v. 79, p. 799, 1996.
12. Varela, J.A.; Cerri, J.A.; Leite, E.R.; Longo, E.; Shamsuzzoha, M.; Bradt, R.C. *Ceram. Intern.*, v. 25, p. 253, 1999.
13. Leite, E.R.; Nascimento, A.M.; Bueno, P.R.; Longo, E.; Varela, J.A. *J. Mat. Sci.: Mat. Electron.*, v. 10, p. 321, 1999.
14. Yongjun, W.; Jinfeng, W.; Hongcun, C.; Weilie, Z.; Peilin, Z.; Huomin, D.; Lianyi, Z. *J. Phys. D: Appl. Phys.*, v. 33, p. 96, 2000.
15. Bueno, P.R.; Leite, E.R.; Oliveira, M.M.; Orlandi, M.O. *Appl. Phys. Lett.*, v. 79, p. 48, 2001.